

# Dynamical Fates of S-Type Planetary Systems in Embedded Cluster Environments

ELIZABETH A. ELLITHORPE<sup>1</sup> AND NATHAN A. KAIB<sup>1,2</sup>

<sup>1</sup>*HL Dodge Department of Physics & Astronomy, University of Oklahoma, Norman, OK 73019, USA*

<sup>2</sup>*corresponding author: nathan.kaib@ou.edu*

## ABSTRACT

The majority of binary star systems that host exoplanets will spend the first portion of their lives within a star-forming cluster that may drive dynamical evolution of the binary-planet system. We perform numerical simulations of S-type planets, with masses and orbital architecture analogous to the solar system’s 4 gas giants, orbiting within the influence of a  $0.5 M_{\odot}$  binary companion. The binary-planet system is integrated simultaneously with an embedded stellar cluster environment.  $\sim 10\%$  of our planetary systems are destabilized when perturbations from our cluster environment drive the binary periastron toward the planets. This destabilization occurs despite all of our systems being initialized with binary orbits that would allow stable planets in the absence of the cluster. The planet-planet scattering triggered in our systems typically results in the loss of lower mass planets and the excitement of the eccentricities of surviving higher mass planets. Many of our planetary systems that go unstable also lose their binary companions prior to cluster dispersal and can therefore masquerade as hosts of eccentric exoplanets that have spent their entire histories as isolated stars. The cluster-driven binary orbital evolution in our simulations can also generate planetary systems with misaligned spin-orbit angles. This is typically done as the planetary system precesses as a rigid disk under the influence of an inclined binary, and those systems with the highest spin-orbit angles should often retain their binary companion and possess multiple surviving planets.

Keywords: stars: binaries: general, planets and satellites: dynamical evolution and stability, galaxies: star clusters: general.

## 1. BACKGROUND & MOTIVATION

The dynamics of planetary systems serve as signposts of their formation and subsequent evolution. Thus the study of dynamical modeling of exoplanets can be thought of as analogous to archaeology: using both observations and simulations of existing stable planets, we can walk back in time to discover which physical processes govern the behavior of extrasolar worlds. Dynamics offers a strong union of computational and observational astronomy, where an influx of exoplanet observational data has dovetailed nicely with a surge in advancements in numerical algorithms over the last two decades.

It has been long thought that most stars spend some of their early lives in a cluster environment, a large scale body of gas that acts as a stellar nursery that condenses into pre-stellar cores in the gas and dust (Lada & Lada 2003). Recent work (Sadavoy & Stahler 2017) has also bolstered the theory (Kroupa 1995) that the majority of stars are born in a stellar multiple, with their dense pre-stellar cores mutually bound together in a dusty envelope. These multiple bound cores, likely formed via fragmentation (Bonnell & Bate 1994; Bate et al. 2003; Turk et al. 2009), either stay together in a binary as interactions with their gaseous disk decrease the separation between the pair (Bate 2000; Bate et al. 2003), or are pulled apart by a cluster environment (Kroupa 2001). While clusters can unbind so-called ‘soft binaries’ (Kroupa 2001), dynamical interactions with a cluster are not sufficient to explain the observed period distribution of binary stars. Thus, their nascent orbital architecture results from the fragmentation process and interactions with a circumstellar disk early on in their lives (Kroupa & Burkert 2001), and should be considered when we discuss the formation and the dynamics of planets in a holistic manner.

While planets in a binary system have been previously studied in depth with N-body integration, the binary that interacts with the planets is for the most part unperturbed by outside forces (e.g. Holman & Wiegert 1999; Haghighipour & Raymond 2007), or, if the binary is modeled in a cluster, planets are not included (e.g. Kroupa & Burkert 2001).

Similarly, planetary systems as they might interact with a cluster environment have been modeled, but often with mock fly-bys of a star rather than a fully evolved cluster (e.g. [Reche et al. 2009](#); [Cattolico & Capuzzo-Dolcetta 2020](#)). A union of these two simultaneous phenomena, a binary’s effect on planets and a cluster’s effect on a binary, is necessitated by the ubiquitous nature of these interactions in young systems. With N-body simulations produced by hybrid symplectic integration scheme, we offer a new perspective at this complex problem.

The presence of a binary companion has been considered in studies of planetary formation since the 1960’s. Early treatments of planetary stability in a binary system worked within the framework of the restricted 3-body problem ([Huang 1960](#)) and numerical estimates based on analytic models ([Heppenheimer 1978](#)). Early work established that both the formation and the stability of planets in a binary system were possible. Later on, numerical integration to evolve these systems began in earnest, owing largely to developments in symplectic integration methods (e.g. [Wisdom & Holman 1991](#)) that allowed for efficient integrations of entire planetary systems in the presence of a binary. The main question that arises in such a system is in what cases does a binary companion preclude the existence of stable planets. An early work that used the Wisdom-Holman scheme is the exploration of the Alpha Centauri system in [Wiegert & Holman \(1997\)](#), in which the authors used N-body integrations in the [Wisdom & Holman \(1991\)](#) scheme to assess the stability of test particles in and around the Alpha Centauri triplet.

The seminal works in the field of planetary stability in a binary system are [Dvorak \(1986\)](#) and [Holman & Wiegert \(1999\)](#). [Dvorak \(1986\)](#) looked at integrating systems of test particles in the restricted 3-body problem with the Lie series method ([Delva 1985](#)) and established an upper and lower critical orbit that began mapping a region of stability for a planet based on the eccentricity of the binary system. [Dvorak \(1986\)](#) looked at various eccentricities of the binary companion, but in all cases the mass of the binary and the central star were the same. [Holman & Wiegert \(1999\)](#) further built upon this stability analysis via symplectically integrating binary systems with both P-type (where the planet orbits around a binary star pair) and S-type planets (where planets are bound to a single star with a binary companion exterior to their orbit). They produced an analytic form of a planet’s critical orbit based on both the eccentricity of the binary and the stellar mass ratio. Also drawing on [Wisdom & Holman \(1991\)](#) is the work described in [Innanen et al. \(1997\)](#), in which the solar system is integrated in the presence of a binary. The authors exemplified the Kozai effect ([Kozai 1962](#)) in which an inclined binary exchanges angular momentum with the planets, and also showed that the planets can evolve in concert as a rigid disk. This work revealed that the Kozai effect is a pathway that can lead to increased eccentricity of planets. Another analysis of the Kozai effect on planetary stability that takes a different, secular approach is [Fabrycky & Tremaine \(2007\)](#), in which the authors integrated the motion of planets in the presence of a binary to show that tidal friction can circularize an orbit made eccentric by an inclined binary companion.

The stability analysis of [Holman & Wiegert \(1999\)](#) remains of interest to this day, with recent work such as [Lam & Kipping \(2018\)](#) further refining their original critical orbit with a neural network and integrations performed in the publicly available REBOUND integrator ([Rein & Liu 2012](#)). [Quarles & Lissauer \(2018\)](#) also further examined the stability of planets in the presence of a stellar binary, focusing in particular on the planetary architectures appropriate for orbital stability in the  $\alpha$  Centauri system. Analysis of planets in binaries continued with work in [Chambers et al. \(2002\)](#) in which the authors used a mixed variable symplectic method to analyze planetary accretion both in a system where the planetary bodies orbit a primary and are perturbed by a distant binary and one in which they orbit around the binary system in its entirety. While [Chambers et al. \(2002\)](#) utilized an integrator that allows for the presence of a binary, further work by [Beust \(2003\)](#) introduced a symplectic scheme based on the [Wisdom & Holman \(1991\)](#) method, called Hierarchical Jacobian Symplectic (HJS), that allows for the integration of a multiple system of any size (i.e., numbering more massive bodies than just a binary) as long as there is a retained hierarchy among the masses. The presence of a distant companion has also been considered in numerical integrations of protoplanetary (debris) disks. [Reche et al. \(2009\)](#) used the HJS scheme to integrate the HD141596 triple star system and debris disk in the presence of stellar flybys. [Beust et al. \(2014\)](#) used symplectic integration to model the Fomalhaut triplet in addition to its dust belt.

On the larger scale, N-body simulations of stellar clusters have been used to study how stellar binaries interact with a cluster environment. [Bate et al. \(2003\)](#) used high resolution simulations of a collapsing gas cloud to study the fragmentation of gas into dense cores, and the subsequent evolution of these young stars into binaries. They found that very tight binaries are formed by the hardening of wider binaries via dynamical interactions. [Adams et al. \(2006\)](#) and [Proszkow & Adams \(2009\)](#) used N-body simulations of moderately sized stellar clusters (100-10,000 members) or embedded clusters to study the impact of a cluster environment on planet formation, particularly in how protoplanetary

disks may be affected by stellar radiation. They found that disruption of model solar systems in an evolved cluster environment (Adams et al. 2006) should be relatively rare due to the paucity of encounters between a ‘solar system’ in question and a passing star, but in younger, denser clusters the photoevaporation of disks by a cluster environment can be appreciable (Proszkow & Adams 2009).

Also addressing the evolution of a stellar cluster is work by Parker & Goodwin (2009) and Parker et al. (2009) in which N-body simulations are used to analyze the prevalence of planets susceptible to the Kozai effect from a binary companion, and the stability of binaries in a dense cluster environment respectively. Parker & Goodwin (2009) found that around 20% of all exoplanets should at one point in their lives be in the presence of a binary companion that has been sufficiently inclined by its cluster environment such that Kozai cycles can occur. This is an intriguing finding that bolsters the idea that a binary companion perturbed by the cluster can have an appreciable affect on the planets, with the caveat that the authors only examined the evolution of binary orbits, as their simulations lacked planetary bodies. Additionally, they particularly focused on very dense clusters similar to Orion, with a half-mass radius of only 0.1 pc. This is not typical for embedded clusters, which have typical half mass radii of  $\sim 0.8$  pc (Lada & Lada 2003), and therefore would have less frequent interactions between cluster stars and a particular binary. Nevertheless, they showed that a dense cluster environment can significantly alter the architecture of a stellar binary which in turn can affect a protoplanetary disk or mature planet system. Parker et al. (2009) focused on similarly dense cluster environments, but instead explored the longevity of moderately wide ( $\sim 10^3$  au) to ultrawide ( $> 10^4$  au) binaries. They found that cluster environments strip away all ultra-wide binary companions, and that the denser clusters, with half mass radii of 0.1–0.2 pc do not retain any binaries with separations  $> 10^3$  au. The less dense clusters, with half mass radii 0.4–0.8 pc, do retain some of these moderately wide binaries. The authors noted that as ultrawide binaries are often stripped in only a few cluster crossing times, these very separated binaries may form in isolation. An alternate channel is that ultrawide binaries are formed during cluster dissolution (Kouwenhoven et al. 2010).

Hao et al. (2013) takes a monte carlo approach to simulating planetary systems in an open cluster to explore planet-planet scattering. The authors modeled stellar flybys and found that multi-planet systems are more sensitive to an open cluster environment than single planet systems. In the realm of exploring planetary orbits in clusters via a model stellar fly-by is work by Malmberg et al. (2011) and Breslau & Pfalzner (2019). Malmberg et al. (2011) showed that fly-bys increase the chance of planetary ejection, while Breslau & Pfalzner (2019) showed that a cluster star can create a retrograde planetary orbit.

In summary, while there is an extensive body of work on the integration of planets in a binary system and the evolution of planets in a cluster environment, previous work largely assumes that the binary is in isolation and does not evolve due to external forces; work concerning cluster environments either model interactions as a flyby or do not include a simultaneous binary system. The work we present here is novel in its approach in that it allows the binary companion to be altered by a cluster environment, and that we fully integrate the passages from and evolution of the cluster rather than taking a flyby approach.

We are largely concerned with the overall fate of binary systems and their planets during these interactions with the cluster. We find that encounters between the binary system and clusters stars can destabilize planets and occur at a non-negligible rate. Moreover, our work has also revealed some intriguing changes in orbital architecture of planetary systems that have a close encounter with an excited binary companion. The remainder of this paper is laid out into the following sections: Section 2 describes how we approach the numerical integration of these systems as well as how we set up the explored parameter space. Section 3 details our findings from these simulations focusing on the mechanism and rate of planetary destabilizations. We then examine the aftermath of systems that have undergone a planetary instability in Section 4, highlighting potential tracers of instability and discussing the broader implications of our results. Finally, we summarize our conclusions in Section 5.

## 2. METHODS

The numerical integrator we use for this work is built on the foundation of the original *Mercury* package (Chambers 1999; Chambers et al. 2002) but with changes to allow the inclusion of multiple bound stellar mass bodies (i.e., a binary or triplet star system) and unbound stellar mass bodies (i.e. stars in a cluster environment). The details of the changes to the integrator are explained in Kaib et al. (2018). We still use the democratic heliocentric coordinates for the planetary system, but the binary is defined relative to the center of mass of the planetary system, and the cluster stars are defined simply with their inertial coordinates. By letting the different bodies be treated with different coordinate systems, this version of *Mercury* retains the advantages of a pure symplectic integrator while still being

able to evolve the unbound cluster stars. That is, there is not a build up of energy error, the pseudo-Keplerian nature of the planetary system integration is retained, and simultaneously the cluster stars and their close approaches can be integrated efficiently in a leapfrog-like scheme.

### 2.1. Simulation Algorithm

In this integration scheme, we define 3 distinct types of bodies: planets bound to the primary, the binary companion, and cluster stars. The cluster star positions are treated with their inertial coordinates, measured only with respect to the cluster's center of mass. The binary's position is integrated with respect to the center of mass of the primary star system (Chambers et al. 2002). The planets are integrated in democratic heliocentric coordinates with respect to the primary star (Duncan et al. 1998). The choice of these coordinates means that the cluster stars are integrated with a purely symplectic  $T + V$  leapfrog scheme. This conserves energy and angular momentum, and is quite accurate as the timescale of cluster stars orbiting in the cluster is much larger than the simulation time step set by the orbits of the planetary bodies. The binary and the planets are also integrated symplectically, although with a mixed variable symplectic Wisdom-Holman scheme (Wisdom & Holman 1991). Finally, when interacting bodies near each other and non-Keplerian terms in the Hamiltonian become comparatively large, the bodies are integrated directly with a Bulirsch-Stoer scheme (Chambers 1999). For the planets, this occurs when passing within a Hill radius of one another. For cluster stars with much larger spheres of influence, the changeover to a direct integration occurs when two stars are close enough to one another that their free fall time is less than  $500\times$  the simulation time-step of 100 days. For a  $1 M_\odot$  star, this corresponds to a close encounter distance of  $\sim 130$  au.

Thus, this scheme largely preserves the angular momentum and energy conservation of a symplectic scheme while allowing for close encounters. Equation 1 shows how we define the position of each type of object, where  $\vec{X}_A$  represents the position of the primary star,  $\vec{X}_B$  the position of the binary,  $\vec{X}_i$  for  $1 \leq i \leq N_P$  is the position of a planet, and  $\vec{X}_i$  for  $N_P < i \leq N_P + N_S$  is the position of a cluster star. The lowercase  $\vec{x}$  represents each type of body's inertial coordinates relative to the origin/center of mass of the cluster.

$$\begin{aligned}
 \vec{X}_A &= \frac{m_A \vec{x}_A + m_B \vec{x}_B + \sum_{j=1}^{N_P} m_j \vec{x}_j}{m_A + m_B + \sum_{j=1}^{N_P} m_j} \\
 \vec{X}_i &= \vec{x}_i - \vec{x}_A \text{ for } 1 \leq i \leq N_P \\
 \vec{X}_B &= \vec{x}_B - \frac{m_A \vec{x}_A + \sum_{j=1}^{N_P} m_j \vec{x}_j}{m_A + \sum_{j=1}^{N_P} m_j} \\
 \vec{X}_i &= \vec{x}_i \text{ for } N_P < i \leq N_P + N_S
 \end{aligned} \tag{1}$$

As such, we define some useful position vectors for changing between reference frames.  $\vec{s}$  marks the barycenter of the planets relative to the primary host star and  $\vec{\Delta}$  marks the inertial position of the primary star as defined with the new coordinates ( $\vec{X}$ 's).

$$\begin{aligned}
 \vec{s} &= \frac{\sum_{i=1}^{N_P} m_i \vec{X}_i}{m_A + \sum_{i=1}^{N_P} m_i} \\
 \vec{\Delta} &= \vec{X}_A - \frac{\sum_{i=1}^{N_P} m_i \vec{X}_i + m_B (\vec{X}_B + \vec{s})}{m_A + m_B + \sum_{i=1}^{N_P} m_i}
 \end{aligned} \tag{2}$$

The corresponding conjugate momenta for the bodies is as follows, again where the lowercase terms are for the inertial case and the uppercase terms are the momenta for the new coordinates:

$$\begin{aligned}
\vec{P}_A &= \vec{p}_A + \vec{p}_B + \sum_{j=1}^{N_P} \vec{p}_j \\
\vec{P}_i &= \vec{p}_i - m_i \frac{\vec{p}_A + \sum_{j=1}^{N_P} \vec{p}_j}{m_A + \sum_{j=1}^{N_P} m_j} \text{ for } 1 \leq i \leq N_P \\
\vec{P}_B &= \vec{p}_B - m_B \frac{\vec{p}_A + \vec{p}_B + \sum_{j=1}^{N_P} \vec{p}_j}{m_A + m_B + \sum_{j=1}^{N_P} m_j} \\
\vec{P}_i &= \vec{p}_i \text{ for } N_P < i \leq N_P + N_S
\end{aligned} \tag{3}$$

In this symplectic scheme, we must consider how Hamilton's equations evolve for all members of the system. We consider mutual gravitation between the primary star, binary star, planets and cluster stars. We also consider the gravitational tide from the gas of the Plummer potential (Plummer 1911) that we assume to be binding the cluster stars together. We include the derivation for the Plummer potential here. We treat the force from a Plummer distribution as a constant background potential whose origin is the center of mass of the cluster stars. As the effect of the Plummer potential is dependent on the inertial position of each massive body within the cluster, the calculation in our chosen (non-inertial) coordinates is fairly complicated. The expression for the force from the sphere of gas is different for each type of body, namely the planets, the binary, and the cluster stars. We begin with the expression for the mass distribution of a Plummer sphere in inertial coordinates, where  $\vec{x}$  is defined relative to the cluster's center-of-mass.

$$\rho(\vec{x}) = \frac{3M_0}{4\pi a_0} \times \left(1 + \frac{|\vec{x}|^2}{a_0^2}\right)^{-5/2} \tag{4}$$

This mass distribution, where  $M_0$  is the total mass in gas of the Plummer sphere and  $a_0$  is a scale parameter that sets the size of the flat core region results in a gravitational potential of:

$$\Phi(\vec{x}) = -\frac{GM_0}{(|\vec{x}|^2 + a_0^2)^{1/2}} \tag{5}$$

The potential energy of our system can then be written as:

$$\begin{aligned}
V_{Plum} &= - \sum_{i=N_P+1}^{N_P+N_S} \frac{GM_0 m_i}{(|\vec{X}_i|^2 + a_0^2)^{1/2}} - \sum_{i=1}^{N_P} \frac{GM_0 m_i}{(|(\vec{\Delta} + \vec{X}_i)|^2 + a_0^2)^{1/2}} \\
&\quad - \frac{GM_0 m_B}{(|(\vec{\Delta} + \vec{s} + \vec{X}_B)|^2 + a_0^2)^{1/2}} - \frac{GM_0 m_A}{(|\vec{\Delta}|^2 + a_0^2)^{1/2}}
\end{aligned} \tag{6}$$

For clarification, the inertial position with which the strength of the Plummer potential is measured in simulation coordinates is  $\vec{X}_i$  for the cluster stars,  $\vec{\Delta} + \vec{X}_i$  for the planets,  $\vec{\Delta} + \vec{s} + \vec{X}_B$  for the binary, and  $\vec{\Delta}$  for the primary. We can then calculate the acceleration due to the Plummer sphere on each body (indexed with  $i$ ) for each cartesian coordinate (indexed with  $u$ ) via:

$$m_i \frac{dv_{i,u}}{dt} = -\frac{\partial V_{plum}}{\partial x_{i,u}} \tag{7}$$

### 2.1.1. Cluster Stars

The positions of the cluster stars in the integration coordinates are exactly their inertial coordinates in this integration scheme (i.e., they are measured relative to the origin). This makes finding the acceleration due to the Plummer tide much more straightforward than for the planets and the binary star pair:

$$\vec{X}_i = \vec{x}_i \text{ for } i > N_P \tag{8}$$

$$\frac{dv_{i,u}}{dt} = -\frac{GM_0 X_{i,u}}{(|\vec{X}_i|^2 + a_0^2)^{3/2}} \quad (9)$$

We can see that the acceleration due to the Plummer sphere on the cluster stars is simply a direct term based on the mass of the gas enclosed by the cluster star's current position.

### 2.1.2. Planets

Recall that  $\vec{\Delta}$  is a function of the position of the planets.

$$\frac{\partial \vec{\Delta}}{\partial X_i} = -m_i \frac{1}{m_A + \sum_{k=1}^{N_P} m_k} \quad (10)$$

This dependence on the planets' positions leads to a more complicated expression for the Plummer potential on the planetary bodies.

$$\begin{aligned} \frac{dv_{i,u}}{dt} = \frac{GM_0}{m_A + \sum_{j=1}^{N_P} m_j} & \left[ \sum_{k=1}^{N_P} \frac{m_k(\Delta_u + X_{k,u})}{(|\vec{\Delta} + \vec{X}_k|^2 + a_0^2)^{3/2}} + \frac{m_A \Delta_u}{(|\vec{\Delta}|^2 + a_0^2)^{3/2}} \right] \\ & - \frac{GM_0(\Delta_u + X_{i,u})}{(|\vec{\Delta} + \vec{X}_i|^2 + a_0^2)^{3/2}} \end{aligned} \quad (11)$$

### 2.1.3. Binary Companion

The vector  $\vec{\Delta}$  is also a function of the position of the binary:

$$\frac{\partial \vec{\Delta}}{\partial X_B} = \frac{-m_B}{m_A + m_B + \sum_{i=1}^{N_P} m_i} \quad (12)$$

Thus, as with the planets, the expression for the acceleration of the binary star due to the Plummer potential is more complicated than what we showed previously for the cluster stars:

$$\begin{aligned} \frac{dv_{B,u}}{dt} = \frac{GM_0}{m_A + m_B + \sum_{j=1}^{N_P} m_j} & \left[ \sum_{k=1}^{N_P} \frac{m_k(\Delta_u + X_{k,u})}{(|\vec{\Delta} + \vec{X}_k|^2 + a_0^2)^{3/2}} \right. \\ & \left. + \frac{X_{B,u} + s_u + \Delta_u}{(|\vec{\Delta} + \vec{X}_B + \vec{s}|^2 + a_0^2)^{3/2}} + \frac{m_A \Delta_u}{(|\vec{\Delta}|^2 + a_0^2)^{3/2}} \right] - \frac{GM_0(X_{B,u} + s_u + \Delta_u)}{(|\vec{\Delta} + \vec{X}_B + \vec{s}|^2 + a_0^2)^{3/2}} \end{aligned} \quad (13)$$

This modified version of the *Mercury* simulation package is publicly available for download at [https://github.com/nathankaib/Mercury\\_StarCluster](https://github.com/nathankaib/Mercury_StarCluster).

## 2.2. Cluster Environments

First, we must decide how to build our stellar clusters. Our clusters consist of many discrete stellar mass bodies embedded within a more massive background Plummer potential to mimic the gravitational effects of a dominant gaseous component to the clusters. To design the parameters of the stellar cluster, we turn to the embedded cluster catalog compiled by Lada & Lada (2003), which Adams et al. (2006) find is mostly comprised of clusters with 100–1000 stars.

While 1000-star clusters begin to have prohibitive runtimes, we employ small, medium, and large cluster environments with 122, 221, and 509 stars, respectively. These have total stellar masses of 80, 160, and 341  $M_\odot$ . In embedded clusters, the stellar mass only represents a small fraction of the total cluster mass, as Lada & Lada (2003) estimate embedded cluster star formation efficiencies between  $\sim 10$ –25%. To bracket the low end of this range, our small and medium clusters have Plummer masses of 1000 and 2000  $M_\odot$ , yielding star formation efficiencies of 7.4%. Meanwhile, our large cluster employs a Plummer mass of 1364  $M_\odot$ , yielding a higher star formation efficiency of 20%. To highlight the role of the non-stellar potential, we also include a version of our medium cluster with all stellar masses reduced by an order of magnitude, implying a star formation efficiency of just 0.74%.



Cluster	Plummer Mass ( $M_{\odot}$ )	Stellar Mass ( $M_{\odot}$ )	Star Formation Efficiency (%)	Plummer Radius (pc)	$N_*$	$\bar{n}_*$ ( $\text{pc}^{-3}$ )
Small	1000	80	7.4	0.62	122	47.4
Medium	2000	160	7.4	0.62	221	86.0
Large	1364	341	20	1.38	541	22.2
NonStellar	2000	16	0.74	0.62	221	86.0

**Table 1.** Parameter summary of simulated cluster environments. From left to right, columns are: environment name, mass of Plummer potential, mass of stellar component, implied star formation efficiency, number of stars, mean volume density of stars inside half-mass radius.

To set the Plummer radii of our potentials (and stellar distributions), we again consult [Lada & Lada \(2003\)](#). Using this catalog, [Adams et al. \(2006\)](#) estimate that 122-, 221-, and 509-star clusters (our small, medium, and large clusters) have typical radii of 0.63–1.1, 0.85–1.5, and 1.3–2.3 pc, respectively. For our small and medium cluster environments, we set our Plummer radius to 0.62 pc, implying a half-mass radius of  $\sim 0.8$  pc. For the large cluster environment, we set the Plummer radius to 1.38 pc, yielding a half-mass radius of 1.8 pc.

Our cluster environment parameters are summarized in Table 1. The goal of this work is to probe a significant swath of cluster parameter space relevant to many planetary systems and not necessarily to the solar system. However, it may be instructive to compare our parameters with constraints on the solar birth cluster, since our work assumes planetary system architectures like our own and it has been speculated that the early Sun may have possessed a binary companion ([Siraj & Loeb 2020](#)). Primarily relying on cluster perturbations to generate the orbit of Sedna while preserving the stability of the giant planets, [Adams \(2010\)](#) concludes that the Sun’s birth cluster contained 1500–7100 stars, or roughly an order of magnitude more than our clusters. However, this assumes a cluster residence time of  $\gtrsim 10$  Myrs. Using the Kuiper belt inclination induced by flybys of cluster stars, [Batygin et al. \(2020\)](#) find that the product of the solar birth cluster residency and stellar density must be below  $\sim 2 \times 10^4 \text{ Myr/pc}^3$ . The values for our clusters are 1–2 orders of magnitude less than this upper limit, so it again appears that much of the allowable parameter space for the solar birth cluster is more populous or denser than our modeled environments.

### 2.3. Simulation Setup and Progression

With cluster parameters specified, our cluster assembly and integration prescription is largely based on the methods outlined in [Levison et al. \(2010\)](#), with some minor differences, as noted below. The masses of the stars are sampled from the [Chabrier \(2003\)](#) piecewise IMF, where we set an upper mass limit of  $150 M_{\odot}$  ([Weidner & Kroupa 2004](#)). Then, the virial speeds of each star are calculated based on their position and we assign them a random initial velocity vector at 8% of the virial speed ([Levison et al. 2010](#)). Once the cluster bodies are positioned following the cluster Plummer profile, we generate different simulations, where for each simulation a random cluster star is converted into the role of the primary, such that the starting position of the planetary/binary system within the cluster is randomized.

A set of 4 gas giants, analogous to the orbits and masses of Jupiter, Saturn, Uranus, and Neptune, are set around a  $1 M_{\odot}$  primary star, and a coplanar  $0.5 M_{\odot}$  binary companion is added as well. We choose to fix our binary mass at this fiducial subsolar value to limit the number of parameters being simultaneously varied. Higher companion masses will likely enhance the destabilizing power of the binary companion, while lower ones should diminish it.

Before integration within a cluster environment, all of our planet+binary systems are first verified via numerical integration to be inherently stable for 10 Myr in isolation. If they are not stable, the initial conditions are discarded. If they do prove to be stable, they are then integrated for 10 Myrs within the cluster environment in concert with all of the other cluster stars. After 5 Myrs of this 10-Myr integration, the Plummer potential is instantaneously dispersed, leaving only the stars and planets. This corresponds to the physical dispersal of the cluster gas, and past modeling works have employed similar dispersal timescales ([Adams et al. 2006](#); [Proszkow & Adams 2009](#); [Levison et al. 2010](#); [Brasser et al. 2012](#)).

### 2.4. Binary Orbits

The influence of the binary on our planetary systems and its susceptibility to perturbation from our cluster environments of course strongly depends on its orbit. Our choices for binary orbits vary across our different sets of simulations. To initially limit the number of parameters being varied within a simulation set, we first perform three sets of 600

Name	Cluster Environment	Binary Eccentricities	Binary Semimajor Axes (au)	Number of Simulations
Small_Fixed	Small	$e = 0.5$	300–800	600
Medium_Fixed	Medium	$e = 0.5$	300–800	600
Large_Fixed	Large	$e = 0.5$	300–800	600
Medium_Cold	Medium	$f(e) \propto \sqrt{e}$	300–800	600
Medium_Uniform	Medium	$f(e) \propto e$	300–800	600
Medium_Thermal	Medium	$f(e) \propto e^2$	300–800	600
Medium_Wider	Medium	$f(e) \propto e^2$	900–1300	500
NonStellar_Fixed	NonStellar	$e = 0.5$	300–800	600
NonStellar_Wider	NonStellar	$f(e) \propto e^2$	900–1300	500

**Table 2.** Summary of simulation sets. From left to right, columns are: simulation set name, cluster environment of simulation set (see Table 1), binary eccentricity distribution, and range of binary semimajor axes (spanned in 100 au intervals), and total number of simulations.

simulations in which the binary eccentricity is fixed at 0.5. Meanwhile, in each simulation set, the binary semimajor axes are varied in increments of 100 au between 300 and 800 au, with 100 different simulations (different starting cluster positions) performed at each binary semimajor axis. (For semimajor axes closer than 300 au the planets are typically immediately unstable, and some binaries beyond 800 au begin to dissociate before cluster gas dispersal.) These fixed eccentricity runs allow us to better isolate the importance of binary semimajor axis and cluster environment.

An additional three sets of simulations explicitly study the importance of the binary’s initial eccentricity within the medium cluster environment. The three different sets employ different distributions of binary eccentricity: uniform in  $e$ , uniform in  $e^2$  (a thermalized distribution; [Ambartsumian 1937](#)), and uniform in  $e^{1/2}$ . For each individual simulation, we again first verify that the choice of binary eccentricity between 0 and 1 from the requisite distribution resulted in a system of stable planets for 10 Myr without the presence of the cluster environment. This gave us an approximate upper bound of  $e = 0.8$  for the widest 800 au binaries and  $e = 0.6$  for the tightest 300 au binaries. Especially in the case of simulations where the planets are on the edge of stability, we operate under the assumption that planets can form in the presence of such an eccentric binary companion. This can be physically explained either that we start the 10 Myr simulation at a snapshot where the cluster has perturbed the binary to its high starting eccentricity and we are examining how long the planets remain stable after further perturbations, or that when the planets are forming in a gas disk, the eccentricity perturbations from cluster stars are damped out by the disk material. Either way, we are embedding a system that is stable in isolation, and examining how the cluster affects the binary from that point.

We also run another follow-on set of simulations that explore slightly larger binary semimajor axes. As mentioned earlier, the binary dissociation times decrease with binary semimajor axes. To destabilize the planets from an  $e = 0.5$  starting eccentricity, the binary periastron has to decrease dramatically in a widely separated binary. However, our thermalized runs begin many binaries on higher eccentricities nearer to the point of planetary instability. To study whether more weakly bound binaries could also trigger a planetary system instability, this set of simulations spans binary semimajor axes between 900 and 1300 au in semimajor axis increments of 100 au. These binaries are also immersed in the medium cluster environment described above.

Finally, we perform two more sets of simulations in the reduced stellar mass version of our medium cluster environment. These are meant to explore the importance of the Plummer gas potential to our systems’ dynamics. The first set employs binaries with a fixed eccentricity of 0.5 and semimajor axes from 300–800 au, and the second set employs a thermal binary eccentricity distribution with semimajor axes from 900–1300 au. Our various sets of simulations are summarized in Table 2.

### 3. RESULTS

The rates that planetary systems are destabilized are shown in Table 3. We see no strong dependence on the cluster masses we employ. Amongst our fixed eccentricity binaries, we find that 5.5%, 9.0%, and 7.3% of the systems in our small, medium, and large clusters experience planetary system instabilities (lose at least one planet via collision or ejection). Surprisingly, we also do not observe a strong dependence on initial binary semimajor axis. In Figure 1A, we plot the fraction of planetary systems that undergo an instability as a function of binary semimajor axis for our fixed



Name	Planetary Disruption Rate (%)	Binary Dissociation Rate (%)
Small_Fixed	5.5	8.2
Medium_Fixed	9.0	13.0
Large_Fixed	7.3	8.8
Medium_Cold	6.7	11.5
Medium_Uniform	10.8	12.7
Medium_Thermal	14.5	13.2
Medium_Wider	14.4	22.8
NonStellar_Fixed	2.0	0.3
NonStellar_Wider	8.0	0.8

**Table 3.** Summary of instability rates in our simulation sets. From left to right, columns are: simulation set name, percentage of destabilized planetary systems, and percentage of unbound binary companions.

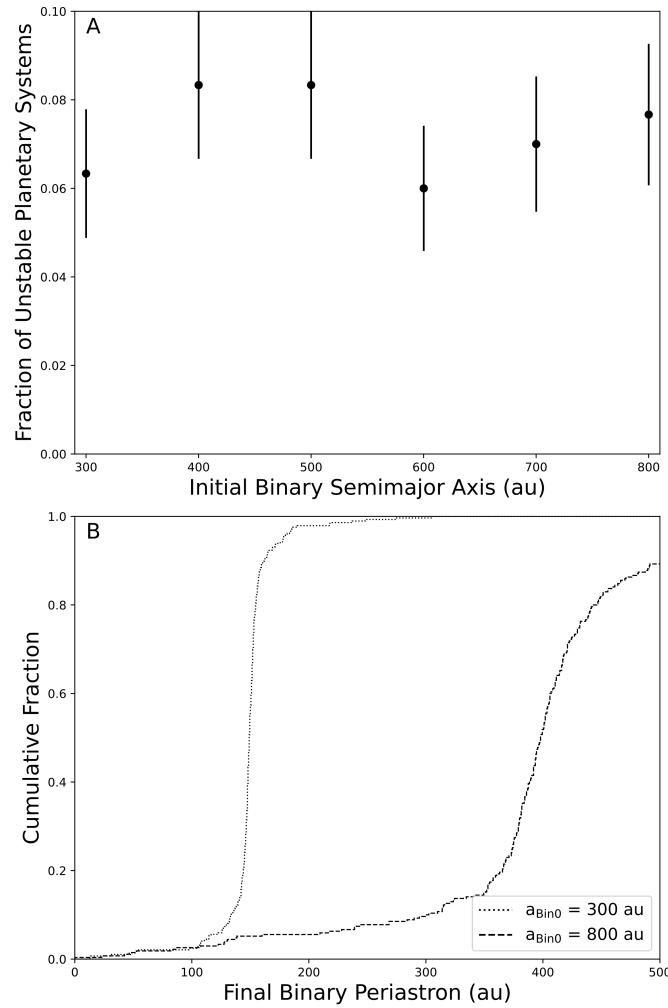


**Figure 1. A:** The fraction of planetary systems that experienced one or more planetary ejections as a function of initial binary semimajor axis with fixed initial binary eccentricity of 0.5. Different cluster mass simulations are co-added and error bars are  $1\sigma$  Poisson uncertainties. **B:** The cumulative distribution of final binary periastra for binaries beginning with  $e = 0.5$ . Distributions are obtained via co-adding all three different cluster mass simulations.

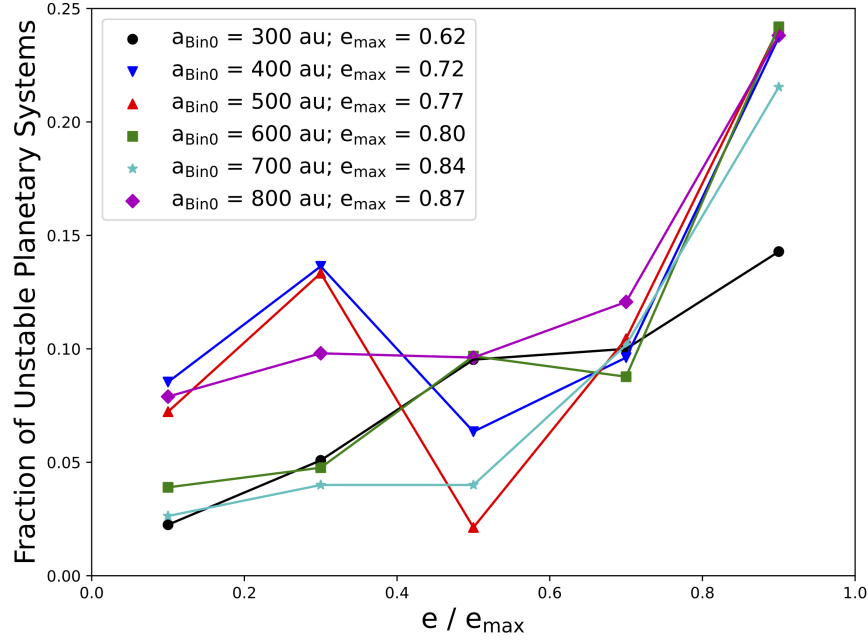


**Figure 2.** Planetary instability rate as a function of initial binary eccentricity (normalized by the maximum initial eccentricity employed for a given binary semimajor axis) in our Medium\_Cold, Medium\_Uniform, and Medium\_Thermal runs. Different lines and symbols correspond to different binary semimajor axes, as detailed in the legend. Legend also lists the maximum initial binary eccentricity for each semimajor axis.

binary eccentricity runs. As can be seen, there is no clear trend across binary semimajor axes of 300–800 au, with instability rates hovering between  $\sim 5$ –9%. We can see why this is the case in Figure 1B, where we examine the final periastron distributions for  $a = 300$  au binaries and  $a = 800$  au binaries. Here we see that the two distributions are radically different, retaining signatures of their identical initial eccentricities but differing semimajor axes. However, at the low periastron tail, the two samples have nearly identical fractions of systems with periastra below  $\sim 100$  au. Coincidentally, periastron passages within 100 au are what are typically capable of destabilizing our planetary systems, where the instability probability quickly falls off for more distant periastron passages. Thus, the greater periastron evolution experienced by our  $a = 800$  au binaries roughly offsets the effects of the lower initial periastra of our  $a = 300$  au binaries.

For our variable eccentricity simulations, we see a clearer sign that instability rates vary with different initial distributions of binary eccentricity. The fraction of planetary instability is 6.7% for the low eccentricity distributions, 10.8% for the uniform case, and 14.5% for the thermalized case, steadily increasing as the initial binary eccentricities are biased toward higher values. We can see this dependence more obviously in Figure 2. Here we co-add the results of our Medium\_Cold, Medium\_Uniform, and Medium\_Thermal runs and then separate them by binary semimajor axis. The fraction of planetary systems that have undergone instability is then plotted against the initial binary eccentricity normalized by the maximum binary eccentricity used for a given binary semimajor axis. (Since we require systems to be stable in isolation, different binary semimajor axes allow for different maximum eccentricities.) This plot demonstrates that the probability of planetary instability increases by a factor of  $\sim 3$ –5 across the range of eccentricities employed for each binary semimajor axis.

Although we see a clear dependence of planetary instability probability on the binary’s eccentricity, we again do not see a strong dependence on binary semimajor axis. Even though some of our wider binaries begin to be dissociated by the end of the cluster’s life and also need to attain a more extreme eccentricity to disrupt their planets, this appears to be roughly offset by the greater orbital variation these binaries incur due to cluster perturbations. This raises the possibility that significant planetary instability rates persist to wider binaries. Our Medium\_Wider simulations suggest that this is the case. Extending the binary semimajor axes from 800 au to 1300 au (using a thermal binary eccentricity distribution), we see no sign of a significant drop off in planetary instability rates, with 14.4% of systems undergoing an instability. This is in spite of the fact that our widest binaries ( $a = 1300$  au) need to typically reach a much more

extreme eccentricity of  $\sim 0.93$  to destabilize the planets compared to our tightest binaries, which only need to typically exceed  $e = 0.62$ .

A unifying factor that we can point to in the case of destabilized systems is the number of close encounters a system has with cluster stars, as the perturbing of the binary by the stochastic motion of the cluster can produce planetary instability. This is what we see in the vast majority of cases: interactions with passing cluster stars drive the binary companion to a very eccentric orbit, allowing for close pericenter passages with the primary and its planets. [Kaib et al. \(2013\)](#) found a similar result in an exploration of wider binaries in the galactic field wherein even distant binary companions can be perturbed to eccentric orbits with close pericenter approaches to an inner planet system. In fact, in our simulations the frequency of close stellar encounters seems to be the most important factor in whether or not a system is destabilized. Unstable systems have a clear preference for multiple, close interactions with cluster stars. This is shown in the histogram in Figure 3, where we count the number of times cluster stars pass within  $10^4$  au of our binary system. A clear takeaway from this figure is that destabilized systems typically experience far more close encounters with stellar cluster members than stable systems. The probability of having a large number of close stellar encounters within the cluster is largely dependent on the positional history of our systems within the cluster environment. For each of our simulations, we measure the distance from the primary to the cluster center-of-mass at each time output. For systems that lose at least one planet, this distance’s median value is over 4 times smaller compared to those that remain stable.

Figure 4 illustrates why a large number of encounters with cluster stars enhances the probability of a planetary instability. The example system shown here retains its binary companion, but it evolves from an initial semi-major axis of  $a = 800$  au to  $a \approx 500$  au. At the same time, the binary periastron evolves from 400 au to under 100 au, leading to strong perturbation of the planetary orbits. During this inwards binary evolution, Jupiter and Saturn are pulled to  $\sim 100^\circ$  inclination (as the binary’s orbital inclination also increases to over  $130^\circ$ ), while Uranus and Neptune are ejected from the system. This particular simulation is a good representative of many common characteristics we observe in unstable systems: 1) the binary star moves inward, and its close periastron approaches drive the loss of the planets. 2) The massive inner planets are the most likely survivors of this event. 3) The remaining bound planets are on altered orbits following the binary’s periastron approach, having both higher inclination and eccentricity on average than their stable counterparts. As frequent close encounters from cluster stars are the main driver in these orbital changes, the architecture of planetary system is largely ‘frozen in’ once the cluster becomes unbound after 5 Myr ([Allen et al. 2007](#)), as the frequency of stellar encounters drops precipitously. A similar lack of stellar encounters when the stars are unbound from the gas was seen in [Adams et al. \(2006\)](#).

In 73% of our destabilized systems, at least one planet is left behind, which is good news for observational signals of these disruption events. This may allow us to make inferences about orbital changes due to binary destabilization processes in surviving exoplanets. Figure 4 suggests that planets surviving these binary-triggered instabilities may reside on exceptionally eccentric and/or inclined orbits.

We can also examine the final fate of the binary companion, and we use our fixed binary eccentricity runs to do so. For unstable systems with higher planetary inclinations, this effect is often tied to a similar change in the binary orbit. Among our unstable systems that retain a binary companion and at least one planet at the end of the simulation, the inner planet has a median inclination of  $38.4^\circ$ . If we just look at the systems with planetary inclinations higher than this median, we find that the final median binary inclination is  $52.1^\circ$ . However, when we look at unstable systems in the bottom half of planetary inclinations, we find a much lower final median binary inclination of just  $12.1^\circ$ .

Of course, not all binary companions remain bound until the end of our simulations. Out of our 1800 fixed eccentricity simulations, binary disruption is relatively rare, with 10% of binaries becoming dissociated. However, amongst systems that underwent an instability, the rate of binary dissociation is much higher at 56%. (This is due to the fact that exceptional numbers of close encounters with cluster stars drive the binary evolution required to trigger a planetary instability.) Thus, for the majority of unstable systems, the binary that perturbed the planets is eventually lost to the cluster. Many single-star exoplanet systems should exist in which the planetary orbital architecture exhibits hallmarks of a violent instability, yet the destabilizing binary companion responsible for this is no longer associated with the system.

It is becoming recognized that the exoplanets with the highest known eccentricities have a higher probability of possessing a stellar companion ([Venner et al. 2021](#)). In fact,  $\sim 50\%$  of exoplanets whose eccentricities exceed 0.8 reside in multi-star systems. Our instabilities triggered by a quickly vacated binary companion may also explain a substantial fraction of the  $\sim 50\%$  of such eccentric exoplanets that are not observed to currently reside in a stellar multiple.

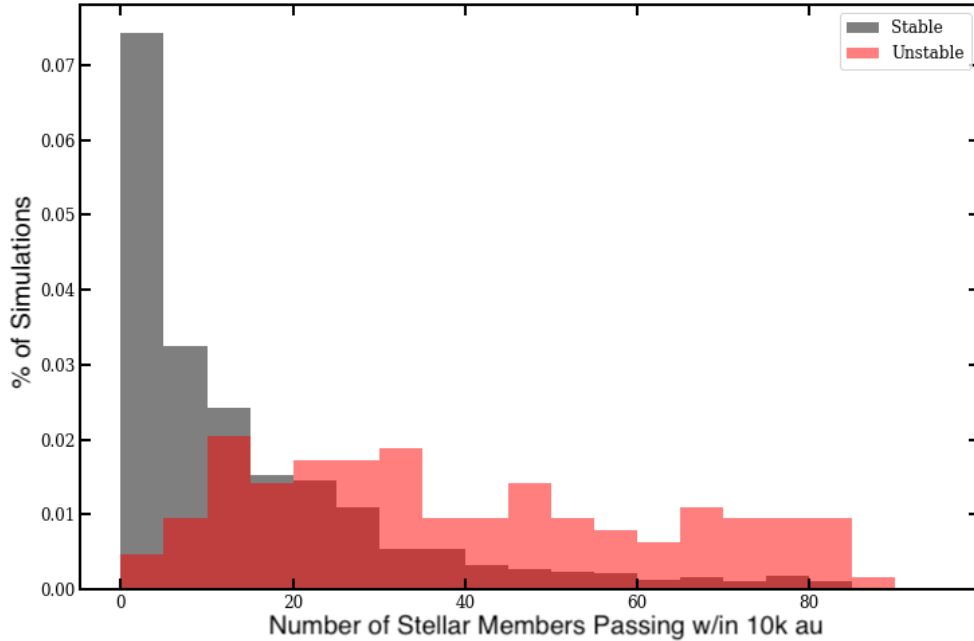


**Figure 3.** A normalized histogram containing results from all 3 suites of simulation depicting the distribution of number of ‘close’ (within 10k au) encounters the planetary system has with cluster stars. The systems with unstable planets are in red, showing a tail of multiple close encounters. The stable systems are shown in black.

## 4. DISCUSSION

### 4.1. *Orbital Architecture Changes*

The orbital architectures of surviving planets in unstable (lose at least one planet) versus stable (retain all four planets) have at least two potentially observable signposts: the eccentricity and spin-orbit angle of the surviving planets. In the following analysis, we take the final planetary orbital inclinations as a proxy for their spin-orbit angles. This makes two implicit assumptions. The first is that the planets are formed on orbits whose angular momentum is aligned with the stellar spin axis. The second is that tidal forces do not subsequently realign the spin axes of our stars with the orbital angular momentum vectors of our planets. Although the sample of known Hot Jupiters with large spin-orbit angles suggests that tidal realignment can occur after spin-orbit angle excitation, the timescale for realignment is not well-constrained, and such timescales would be much longer in our simulated systems whose planets orbit at multiple au (Winn et al. 2010; Hamer & Schlaufman 2022).

The distributions of eccentricity and the predicted spin-orbit angle of the inner gas giants in unstable systems are statistically distinct from their stable counterparts. High eccentricity planets, like the ones we see in our unstable systems, are thought to have a dynamical source. First posited in Rasio & Ford (1996), planet-planet scattering interactions can lead to ejections of some planets and a higher eccentricity for planets that remain. In our systems, often these surviving planets are the two inner gas giants. The Jupiter and Saturn mass planets thus act as good markers of a past instability, and our analysis will focus on their final orbits in each simulation. The distributions of the final eccentricity and inclination of the inner giants are shown in Figure 5. Each of our batches of simulations tells a similar story. The median eccentricities of Jupiter and Saturn analogs in our stable systems are around 0.045, but in systems that have undergone binary-triggered instabilities this median value grows by 50–100%. In addition, a small fraction of unstable systems are driven to more exceptional eccentricities. Depending on the particular simulation batch, 1–3% percent of our surviving gas giants achieve eccentricities above 0.5.

We see similar trends in the evolution of planetary inclinations and assumed spin-orbit angle. In stable systems, the Jupiter and Saturn analogs have a median predicted spin-orbit angle of 2–4°. However, in instability survivors

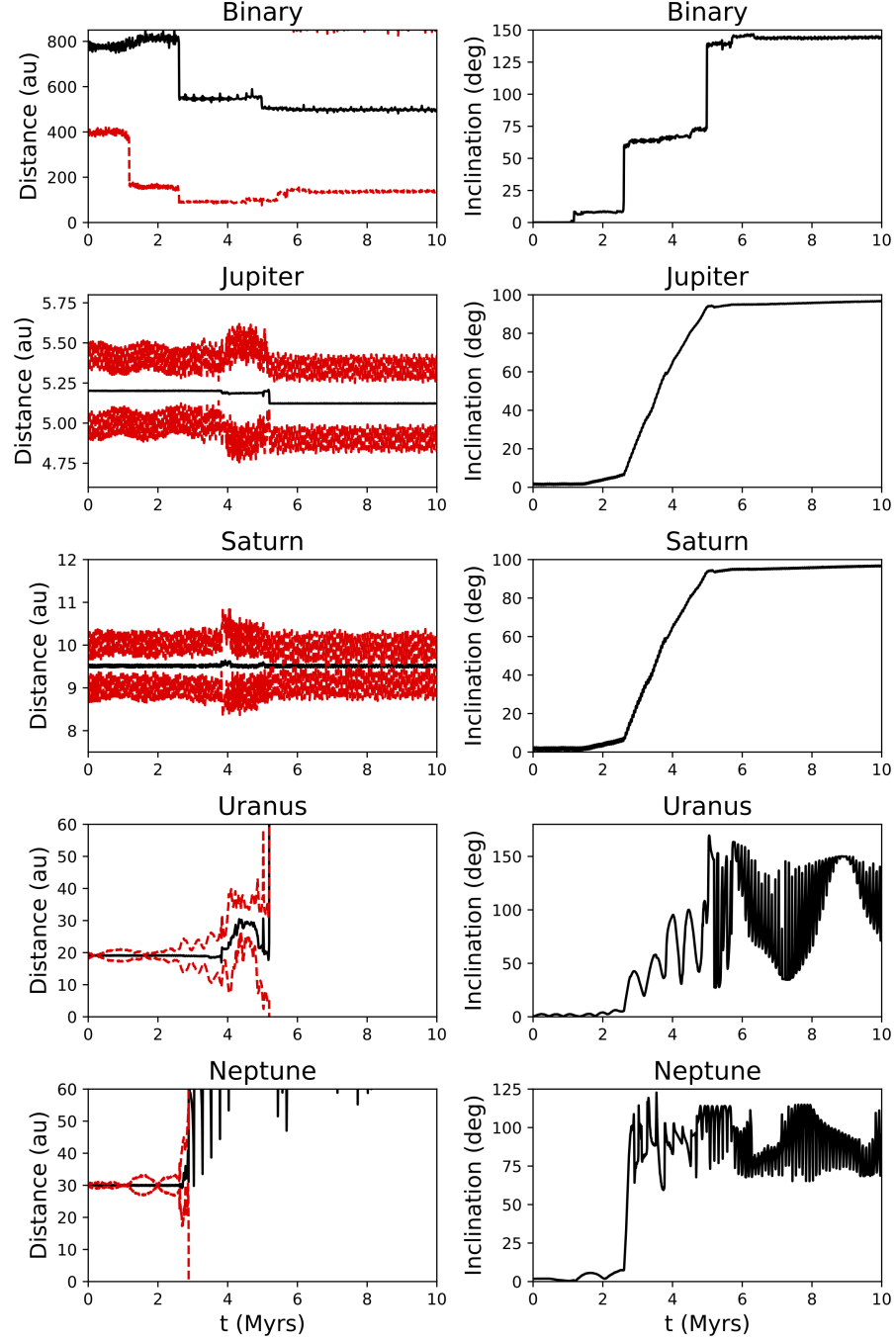


**Figure 4.** The orbital evolution of the 4 giant planets and binary companion. The left panels are the distance of the object from the primary, where the solid black line is the semi-major axis and the dashed red lines are the pericenter/apocenter of the body. This particular system results in a very high predicted spin-orbital angle for the Jupiter and Saturn mass bodies. Note the multiple ‘jumps’ as the binary companion enters a close pericenter approach. These jumps are from encounters with cluster stars in which angular momentum is exchanged. In this simulation both the Uranus and Neptune mass planets become unbound and the binary companion remains bound.

this median value increases to  $15\text{--}30^\circ$ , depending on the particular simulation batch. Often the two inner planets will undergo a coupled evolution as if in a rigid disk (shown in work by [Innanen et al. \(1997\)](#)), reaching similar inclinations after the instability. In addition, approximately 5% of our surviving planets in unstable systems attain spin-orbit angles in excess of  $90^\circ$ .

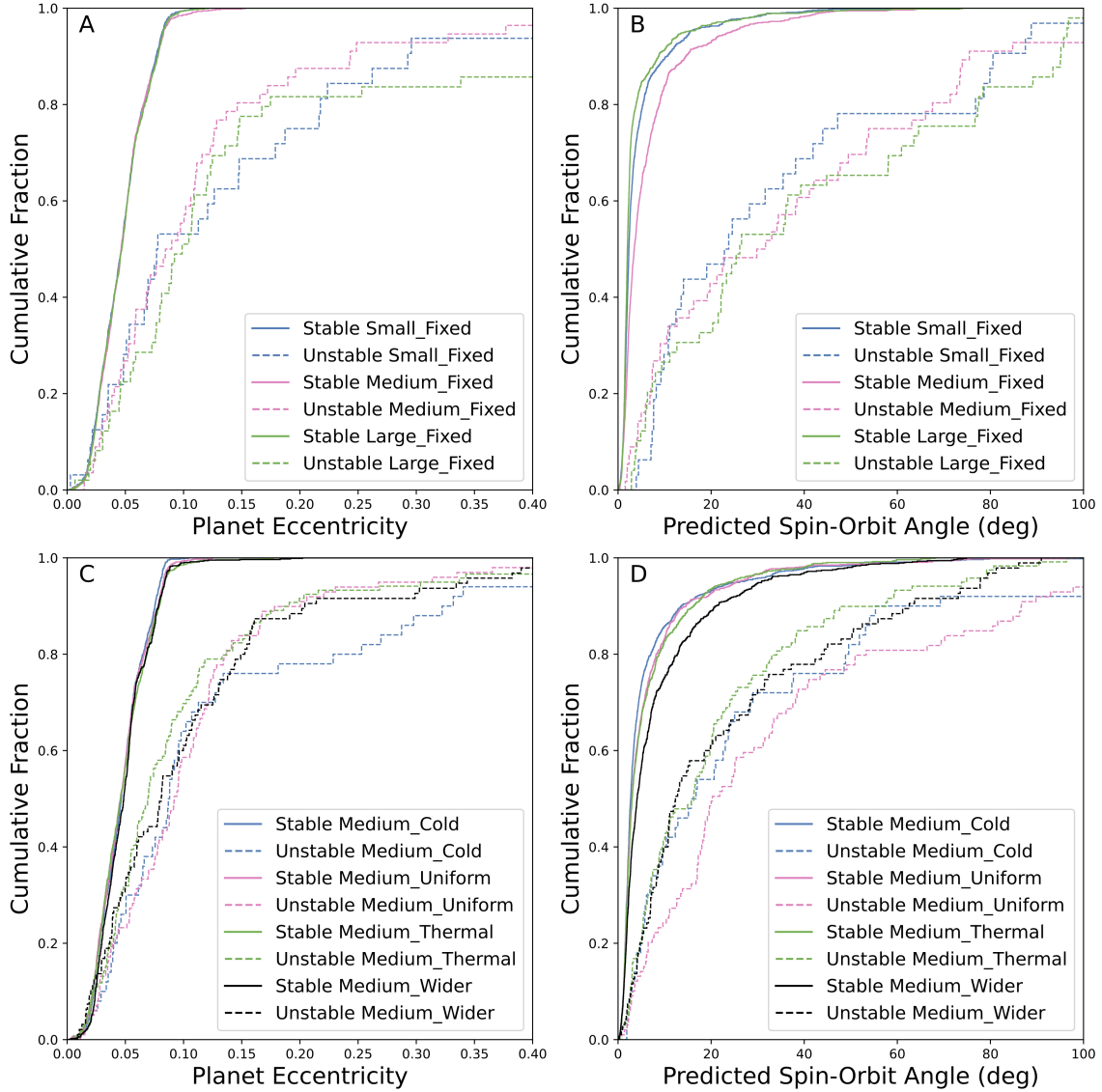


**Figure 5.** **A:** Cumulative distributions of eccentricities of Jupiter and Saturn analogs in stable (solid lines) and unstable (dashed lines) systems from our Small.Fixed, Medium.Fixed, and Large.Fixed simulations. **B:** Cumulative distributions of the predicted spin-orbit angles of the planets from Panel A. **C:** Cumulative distributions of eccentricities of Jupiter and Saturn analogs in stable (solid lines) and unstable (dashed lines) systems from our Medium.Cold, Medium.Uniform, Medium.Thermal, and Medium.Wider simulations. **D:** Cumulative distributions of the predicted spin-orbit angles of the planets from Panel C.

Interactions with the binary companion, whether it remains bound to the primary or not, destabilize the planets via an exchange of orbital angular momentum. If the planets stay bound, this interaction tends to heat up their orbits to higher eccentricities and inclinations. However, when we examine our unstable systems, we find that final planetary inclinations and eccentricities are not particularly strongly correlated ( $r < 0.1$ ). This is because the most common instability leads to the ejection of one or both ice giants, while the Jupiter and Saturn analogs survive. The scattering of ice giants does not necessarily strongly drive the excitation of Jupiter and Saturn analog eccentricities. On the other hand, the binary evolution necessary to trigger ice giant ejections also often elicits significant rigid disk



precession of the Jupiter and Saturn analogs, significantly increasing the spin-orbit angle (Kaib et al. 2011). If we instead limit ourselves to systems that only have 1 surviving planet (nearly always Jupiter after a Saturn ejection), we find a stronger correlation ( $r = 0.37$ ) between final inclination and eccentricity. In addition, the median planetary eccentricity is much higher at 0.25, and this sample also contains 2/3 of our planets that finished with eccentricities above 0.5.

#### 4.2. A Significantly Misaligned Population

If we assume that the planets in our systems begin in an aligned configuration with the stellar spin axis, we can use their orbital inclination as a proxy for the spin-orbit angle  $\Psi$ . We must then consider how the signature of misalignment would be maintained along a hypothetical line of sight. To ensure that the distribution of planetary spin-orbit angles for stable and unstable populations remain distinct, we choose a random observing angle for each system and calculate the projected spin-orbit angle  $\lambda$ . We then can utilize the Kolmogorov-Smirnov test to conclude if we can discard the null hypothesis that the *projected* spin-orbit angles of our stable and unstable systems are drawn from the same parent distribution. We repeat this process of choosing a random viewing angle for each system in the population 100 times, and in all 100 cases we obtain a p-value from our KS test that is less than  $1 \times 10^{-3}$ . Therefore, even when projecting our systems along a hypothetical viewing angle, the distributions remain statistically distinct between stable and unstable systems. A cumulative distribution of this test for our fixed binary eccentricity simulations is shown in Figure 6, where the median value of the projected angle is plotted for the stable and unstable systems and the shaded regions denote the 5<sup>th</sup> and 95<sup>th</sup> percentiles. This N-body gravitational interaction pathway to misalignment is significant, in our simulations, and bolsters the observations that high obliquity planetary systems likely arise from planet scattering events (Winn et al. 2010). Roughly 1/3 of our systems that experienced instability attain projected spin-orbit angles over  $30^\circ$ , while only  $\sim 1/20$  of our stable systems do so.

While our highest eccentricity systems are very likely to be 1-planet systems, this is not the case for our highest inclination planets that have survived instabilities. Of the 16 unstable planetary systems driven to spin-orbit angles over  $90^\circ$ , 12 of them contain both Jupiter and Saturn analogs. In addition, the Jupiter and Saturn analogs in our 12 multi-planet systems all have final inclinations within  $\sim 5^\circ$  of one another (as well as modest eccentricities of  $\lesssim 0.1$ ), indicating that they have attained their high inclinations via rigid disk precession (Innanen et al. 1997).

Also in contrast to planetary eccentricities, there is some correlation between spin-orbit angle and the retention of a binary companion. If we co-add all of our unstable systems and examine those that lost their binary, the median predicted spin-orbit angle is  $11.1^\circ$ . Meanwhile, for those unstable systems that retain their binary, this median angle is over twice as large at  $23.5^\circ$ . This suggests that the retention of the binary leads to continued evolution of planetary inclinations (in particular, rigid disk precession) after the instability.

Given the potentially long timescales for rigid disk precession (see Figure 4 for instance), this raises the prospect that amongst our unstable systems with a binary companion, the spin-orbit inclinations may continue to evolve after our 10-Myr integration times. To test this possibility, we perform follow-on integrations of our unstable systems that possess a binary for another 100 Myrs. The results of these integrations are shown in Figure 7, where we plot their distribution of spin-orbit angles. Here we see that systems with binary companions continue to diverge from those that lost their companions. After the additional 100 Myrs of integration, the median spin-orbit angle has increased from  $23.5^\circ$  to  $33.8^\circ$ . In addition, the fraction of systems with retrograde angles has nearly doubled from 6.5% to 11.1%. (It should be noted that our distribution of spin-orbit angles after 50 Myrs of integration does not exhibit any statistical differences from our 100-Myr sample, suggesting this suite of systems has reached a dynamical equilibrium by the end of its integration.)

This small but significant population of retrograde systems possesses distinct properties. Mostly having achieved their spin-orbit angles via rigid disk precession, the majority (70%) are multi-planet systems with modest eccentricities ( $\bar{e} \simeq 0.09$ ). Such a set of observed systems would be very consistent with a dynamical history where a planetary system is perturbed by a retained binary companion whose orbit is modified within a birth cluster.

#### 4.3. Ramifications for Exoplanets of Single Stars

As mentioned previously, planetary instabilities in our simulations are often accompanied by the dissociation of the binary companion because both processes are tied to strong cluster perturbations on the binary orbit. In fact,  $\sim 41\%$  of our systems that had their binary companion stripped also underwent a planetary orbital instability. Meanwhile, it has been argued that most stars form with one or more stellar companions, but lose their companion via dynamical

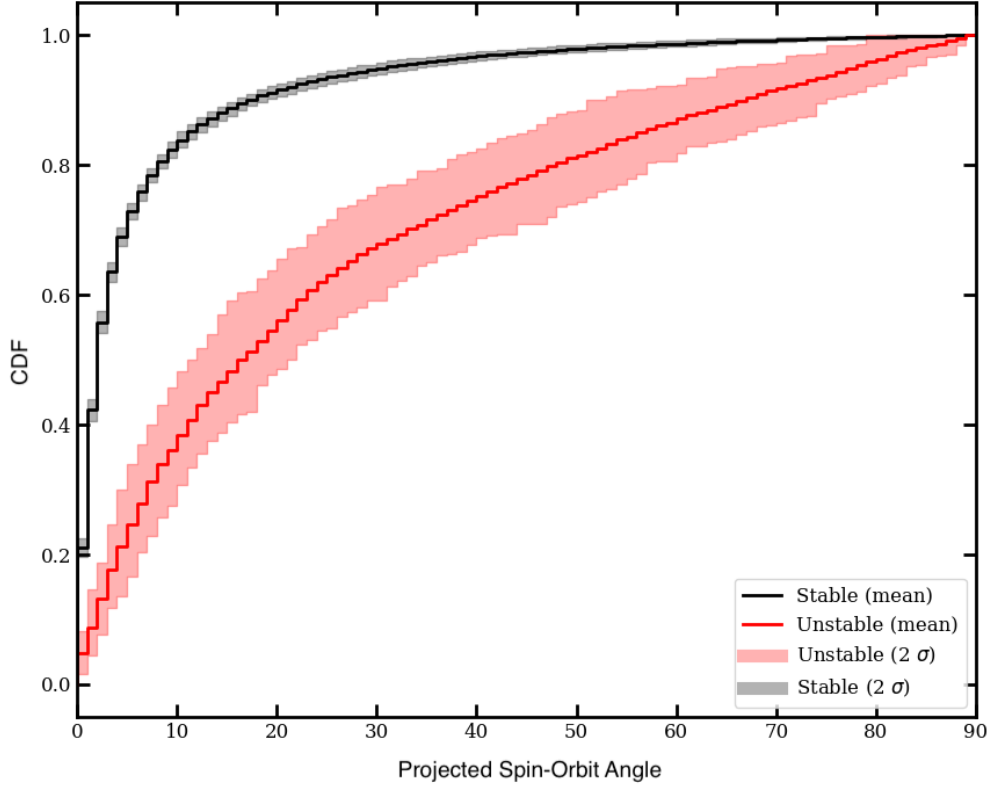


**Figure 6.** Cumulative distributions of the average projected spin-orbit angle after 10 Myrs for stable and unstable systems. Our Small\_Fixed, Medium\_Fixed, and Large\_Fixed simulations are co-added. The shaded regions denote the 5<sup>th</sup> and 95<sup>th</sup> percentiles of projected spin-orbit angle for each bin.

processing (stellar encounters and tidal stripping) within their birth cluster (e.g. Kroupa 1995). Although only a relatively small portion of our simulated systems undergo binary-triggered planetary instabilities (the highest instability rate reached in our simulation sets is  $\sim 15\%$ ), our simulations do not encompass all parameter space of binaries or cluster environments. Moreover, our simulations do not consider substructure within our cluster potentials and make other idealized assumptions such as spherical symmetry and instantaneous dissipation. If the actual physical environments of clusters facilitate higher binary dissociation rates and these processes are responsible for a large fraction of the isolated stars observed in the field, a significant fraction (tens of percent) of planetary systems around isolated stars may be subject to instabilities analogous to those in the simulations we present here.

#### 4.4. The Importance of Gas Potential

The bulk of the mass in our cluster environments is in the form of a Plummer potential meant to represent the gaseous component. On the other hand, Figure 3 demonstrates that encounters with other cluster stars are critical in many of the planetary system instabilities that our simulated binaries trigger, so one may question whether the gas potential is important to the dynamics of this process. To assess this, we perform two simulation sets (NonStellar\_Fixed and NonStellar\_Wider) that are repeats of Medium\_Fixed and Medium\_Wider. Only this time, they are performed in the NonStellar cluster environment in which stellar masses (but not the Plummer mass) are reduced by an order of magnitude.

In Table 3, we see that the rate of planetary instabilities is indeed lower in both reduced stellar mass runs, but the effect is more severe if we use a binary eccentricity distribution fixed at 0.5. Here we find that the instability rate drops by over 75% (from 9% of all systems to 2%). In contrast, when we employ wider binaries with a thermalized

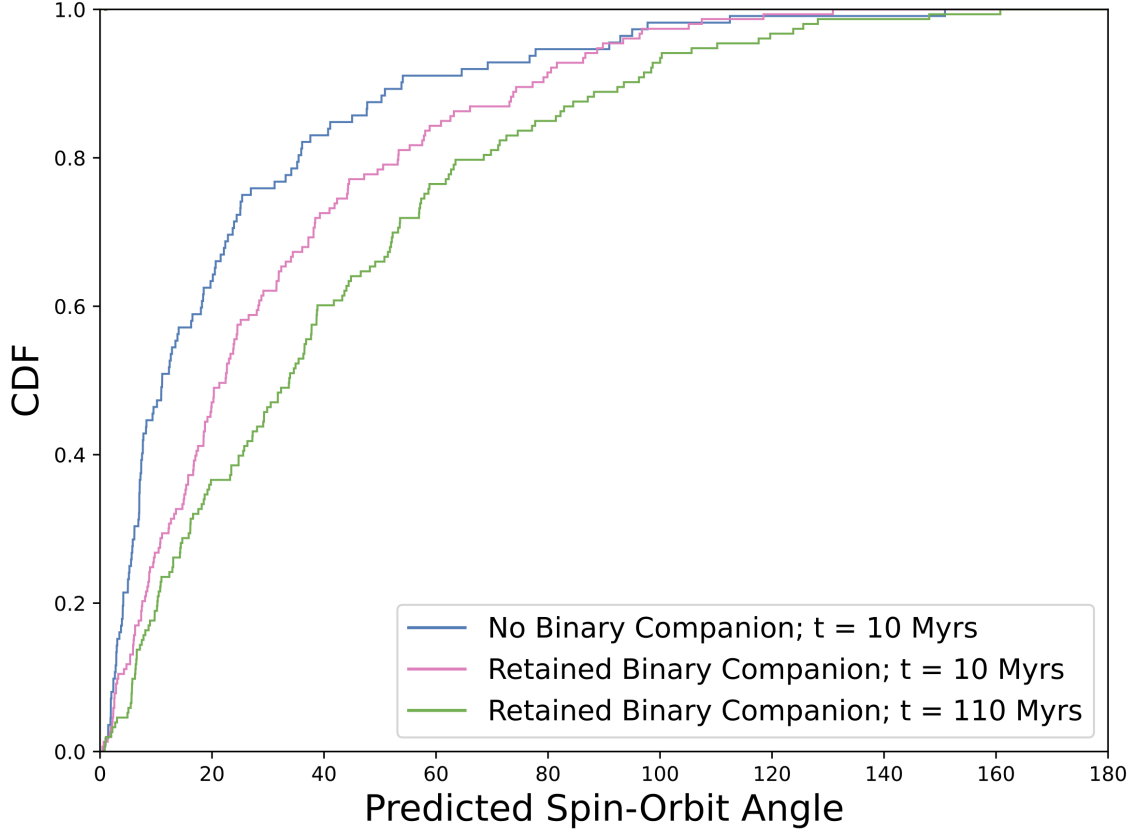


**Figure 7.** Cumulative distributions of the predicted spin-orbit angle for unstable systems (co-added across all simulation batches). Shown are unstable systems that have lost their binary companion (*blue*) and unstable systems that have retained their binary companion after 10 Myrs of integration (*pink*) and 110 Myrs of integration (*green*).

eccentricity distribution there is a more modest decrease in instability rate of 44% (from 14.4% of all systems to 8%). The reason for this more modest change is that our wider binary orbits are more easily perturbed and many more of them are initialized with periastra near values necessary to destabilize our planetary systems. Thus, more systems do not require powerful stellar encounters to dramatically drive periastra low enough for a planetary instability, and this can be accomplished with more modest gaseous perturbations. Thus, the importance of the gas potential increases as one considers more eccentric and more weakly bound binaries.

#### 4.5. Comparison with Past Work

##### 4.5.1. System Stability

As discussed in our introduction, there is an extensive literature studying the stability of planets within binaries and star clusters. Many of the works focused on the stability of planetary systems within clusters only consider the direct effects of stellar flybys, and this limits the rate of planetary instabilities. For instance, [Adams et al. \(2006\)](#) consider the rate that stellar flybys perturb solar system architectures within embedded clusters of 100–1000 stars, and they find only  $\sim 1\%$  of Neptune-like planets around Sun-like stars are destabilized (their Tables 3 and 7). Similarly, [Proszkow & Adams \(2009\)](#) consider an even broader range of cluster parameters and typically find destabilization rates of 0.1–1% for Neptune-like planets (their Table 8). Meanwhile, we show here that the addition of a wide binary companion boosts these destabilization rates by an order of magnitude within comparable cluster environments. To achieve our binary-induced destabilization rates around singleton stars requires much more extreme cluster environments. For instance, [Malmberg et al. \(2011\)](#) find that typical open cluster environments yield a destabilization probability of 5–15% for solar system-like architectures, but their cluster stellar densities are 1–2 orders of magnitude greater than ours, and their cluster lifetimes are 20 times as long. Similarly, [Hao et al. \(2013\)](#) find cluster-generated stellar flybys can disrupt 99% of solar system-like architectures, but to achieve this rate requires cluster densities  $\sim 2$  orders of

magnitude greater than ours and 100-Myr lifetimes. If we examine their disruption rates at 10 Myrs (their Figure 3), it is only  $\sim 2\text{--}10\%$  with, again, a much denser cluster than any of ours. Our simulations show that a wide binary companion acts as a potential conduit allowing perturbations from the cluster environment to greatly boost the rate of planetary instabilities.

Among works studying planetary stability within binaries, many do not consider temporal evolution of the binary orbit. [Holman & Wiegert \(1999\)](#) developed a widely employed empirical formula for the maximum semimajor axis,  $a_c$ , of stable 1-planet systems in the presence of a coplanar wide binary companion with a given mass and eccentricity:

$$a_c = [(0.464 \pm 0.006) + (-0.380 \pm 0.010)\mu + (-0.631 \pm 0.034)e + (0.586 \pm 0.061)\mu e + (0.150 \pm 0.041)e^2 + (-0.198 \pm 0.074)\mu e^2]a_b \quad (14)$$

where  $a_b$  and  $e$  are the binary companion’s semimajor axis and eccentricity, and  $\mu$  is the ratio of the companion mass to the system mass. This formula is approximate (e.g. [Quarles & Lissauer 2018](#)), but if we take Neptune’s semimajor axis of 30 au and note our fixed binary mass ratio of 1/3, it allows us to invert Equation 1 and predict a “critical binary eccentricity” above which our planetary system should be unstable and below which it will be stable:

$$e_c = \frac{.436 - \sqrt{0.19 - 0.336(0.337 - \frac{30}{a_b})}}{0.168} \quad (15)$$

If we then examine our simulated initial binary eccentricities, we find that the vast majority (97.1%) are started on orbits that will allow Neptune to remain stable according to Equation 15. When we examine the 2.9% of binaries whose initial eccentricities exceed  $e_c$  we find that only 1/3 (or less than 1% of our total systems) end up experiencing a planetary instability, underscoring the fact that Equations 14 and 15 are approximate estimates of stability. Thus, without considering cluster-driven binary evolution, a stability analysis of our systems would predict nearly all of our systems to be stable (hence their stability over an isolated integration). However, our simulations record 395 planetary instabilities (9.6% of our integrated systems), and 90% of these unstable systems begin with binary eccentricities below  $e_c$ . Of course, our Medium.Uniform simulation is our only batch of systems with an unskewed binary eccentricity distribution, but if we examine only these systems, we find that 88% of our unstable systems begin below  $e_c$ , and their median initial value is  $0.83e_c$ .

Nearly half of our unstable systems lose their binary companion, but for those that retain it, we can study how the final binary eccentricities compare to  $e_c$ . In these systems, we find that the large majority ( $\sim 80\%$ ) finish with binary eccentricities *above*  $e_c$ . This demonstrates that it is relatively rare in our simulations for binaries to evolve to a destabilizing periastron and then evolve to a more modest periastron after triggering an instability. Our cluster environments tend to disperse before this can occur. Hence, final binary eccentricities relative to Equation 2 are a relatively accurate marker of what types of planets could have been destabilized during the cluster phase. However, these binary orbits should not be taken to conclude that such planets could never have existed early in systems’ histories.

#### 4.5.2. Binary-driven Kozai Cycles

Past work modeling the evolution of binary stars within clusters has noted that cluster perturbations can excite the orbital inclinations of binary stars and initiate Kozai cycles within planetary systems, possibly driving instabilities and planetary eccentricity excitation. [Parker & Goodwin \(2009\)](#) find that  $\sim 20\%$  of binaries can attain inclinations high enough ( $i \gtrsim 40^\circ$ ) to excite planetary Kozai cycles. Our simulations find a comparable fraction; 14.8% of our binary orbits are excited beyond to  $i > 40^\circ$ . However, this is not a guarantee of an instability within our planetary systems. Of those systems whose binary orbit is excited beyond  $i \gtrsim 40^\circ$ , 60% did not experience a planetary instability. This is because Kozai cycles tend to be suppressed in multi-planet systems, and they instead undergo rigid disk precession without substantial eccentricity excitation ([Innanen et al. 1997](#)). Moreover, of our systems that undergo instability and retain a binary, the final binary inclination is below  $40^\circ$  for 60% of systems. This underscores that Kozai cycles are not the primary driver of instability and eccentricity excitation in our multi-planet systems. Instead, it is the periastron evolution of the binary under cluster perturbations (which is sometimes accompanied by significant binary inclination evolution).

## 5. CONCLUSIONS

The simulations we present here demonstrate that wide ( $100 \gtrsim a_b \gtrsim 1000$  au) binary stars likely have an early phase with active temporal orbital evolution while they still inhabit their birth clusters. This binary orbital evolution can in turn destabilize the planetary systems they host, touching off episodes of planet-planet scattering. The instabilities we document are typically triggered as cluster perturbations drive the binary periastron toward the planets, exciting one or more planets onto crossing orbits. Close encounters with other cluster stars are generally the cluster perturbation that modifies the binary orbit, but the tidal potential of cluster gas becomes increasingly relevant as we consider more eccentric and/or more weakly bound binaries. Our simulations display a modest rate of instabilities ranging from 5–15% of all planetary systems. However, due to computational limitations, many regimes of the potential parameter space of embedded star clusters are unexplored. It is possible that other cluster environments as well as different binary and planetary system properties could yield substantially higher rates of planetary instability.

The planetary instabilities that the binaries trigger often cause significant alterations of the planetary architectures. Namely, the lower mass planets (Uranus and Neptune analogs in our case) are preferentially lost, while the surviving planets (typically Jupiter and Saturn analogs) remain with more excited eccentricities. In addition, even though our simulations begin with coplanar binaries, the inclinations of our planets are often altered as well. This is because the same perturbations that alter binary periastra that trigger instabilities also alter binary inclinations. These heightened binary inclinations cause the planetary systems to undergo rigid disk precession (Innanen et al. 1997), which can ultimately lead to high, even retrograde, spin-orbit angles. Notably, it is rigid disk precession, rather than Kozai cycles, that most often generate simulated systems with the highest spin-orbit angles.

In systems with the highest spin-orbit angles, the binary companion that torques the planets is usually retained, but overall, roughly half of our unstable planetary systems also lose their binary, as the cluster perturbations driving binary orbital evolution can lead to binary unbinding. This raises the prospect that some exoplanets with high eccentricities and/or spin-orbit angles around isolated field stars may be the products of cluster-driven evolution of early binary companions that are lost early in the systems’ histories.

## 6. DATA AVAILABILITY STATEMENT

The simulation data underlying this article are available on the Harvard Dataverse public repository.

## 7. ACKNOWLEDGEMENTS

This work was performed with support from NASA Exoplanets Research Program grant 80NSSC19K0445, NSF grant AST-1814762, and NSF CAREER Award 1846388. Our computing was performed at the OU Supercomputing Center for Education & Research (OSCER) at the University of Oklahoma (OU).

## REFERENCES

- Adams, F. C. 2010, *ARA&A*, 48, 47,  
doi: [10.1146/annurev-astro-081309-130830](https://doi.org/10.1146/annurev-astro-081309-130830)
- Adams, F. C., Proszkow, E. M., Fatuzzo, M., & Myers, P. C. 2006, *ApJ*, 641, 504, doi: [10.1086/500393](https://doi.org/10.1086/500393)
- Allen, L., Megeath, S. T., Gutermuth, R., et al. 2007, in *Protostars and Planets V*, ed. B. Reipurth, D. Jewitt, & K. Keil, 361
- Ambartsumian, V. A. 1937, *AZh*, 14, 207
- Bate, M. R. 2000, *MNRAS*, 314, 33,  
doi: [10.1046/j.1365-8711.2000.03333.x](https://doi.org/10.1046/j.1365-8711.2000.03333.x)
- Bate, M. R., Bonnell, I. A., & Bromm, V. 2003, *MNRAS*, 339, 577, doi: [10.1046/j.1365-8711.2003.06210.x](https://doi.org/10.1046/j.1365-8711.2003.06210.x)
- Batygin, K., Adams, F. C., Batygin, Y. K., & Petigura, E. A. 2020, *AJ*, 159, 101, doi: [10.3847/1538-3881/ab665d](https://doi.org/10.3847/1538-3881/ab665d)
- Beust, H. 2003, *A&A*, 400, 1129,  
doi: [10.1051/0004-6361:20030065](https://doi.org/10.1051/0004-6361:20030065)
- Beust, H., Augereau, J. C., Bonsor, A., et al. 2014, *A&A*, 561, A43, doi: [10.1051/0004-6361/201322229](https://doi.org/10.1051/0004-6361/201322229)
- Bonnell, I. A., & Bate, M. R. 1994, *MNRAS*, 271, 999,  
doi: [10.1093/mnras/271.4.999](https://doi.org/10.1093/mnras/271.4.999)
- Brasser, R., Duncan, M. J., Levison, H. F., Schwamb, M. E., & Brown, M. E. 2012, *Icarus*, 217, 1,  
doi: [10.1016/j.icarus.2011.10.012](https://doi.org/10.1016/j.icarus.2011.10.012)
- Breslau, A., & Pfalzner, S. 2019, *A&A*, 621, A101,  
doi: [10.1051/0004-6361/201833729](https://doi.org/10.1051/0004-6361/201833729)
- Cattolico, R. S., & Capuzzo-Dolcetta, R. 2020, *Astrophysics and Space Science*, 365, doi: [10.1007/s10509-020-03885-4](https://doi.org/10.1007/s10509-020-03885-4)
- Chabrier, G. 2003, *Publications of the Astronomical Society of the Pacific*, 115, 763–795, doi: [10.1086/376392](https://doi.org/10.1086/376392)
- Chambers, J. E. 1999, *MNRAS*, 304, 793,  
doi: [10.1046/j.1365-8711.1999.02379.x](https://doi.org/10.1046/j.1365-8711.1999.02379.x)

- Chambers, J. E., Quintana, E. V., Duncan, M. J., & Lissauer, J. J. 2002, *AJ*, 123, 2884, doi: [10.1086/340074](https://doi.org/10.1086/340074)
- Delva, M. 1985, *A&AS*, 60, 277
- Duncan, M. J., Levison, H. F., & Lee, M. H. 1998, *AJ*, 116, 2067, doi: [10.1086/300541](https://doi.org/10.1086/300541)
- Dvorak, R. 1986, *A&A*, 167, 379
- Fabrycky, D., & Tremaine, S. 2007, *ApJ*, 669, 1298, doi: [10.1086/521702](https://doi.org/10.1086/521702)
- Haghighipour, N., & Raymond, S. N. 2007, *ApJ*, 666, 436, doi: [10.1086/520501](https://doi.org/10.1086/520501)
- Hamer, J. H., & Schlaufman, K. C. 2022, arXiv e-prints, arXiv:2205.00040. <https://arxiv.org/abs/2205.00040>
- Hao, W., Kouwenhoven, M. B. N., & Spurzem, R. 2013, *MNRAS*, 433, 867, doi: [10.1093/mnras/stt771](https://doi.org/10.1093/mnras/stt771)
- Heppenheimer, T. A. 1978, *A&A*, 65, 421
- Holman, M. J., & Wiegert, P. A. 1999, *AJ*, 117, 621, doi: [10.1086/300695](https://doi.org/10.1086/300695)
- Huang, S.-S. 1960, *PASP*, 72, 106, doi: [10.1086/127489](https://doi.org/10.1086/127489)
- Innanen, K. A., Zheng, J. Q., Mikkola, S., & Valtonen, M. J. 1997, *AJ*, 113, 1915, doi: [10.1086/118405](https://doi.org/10.1086/118405)
- Kaib, N. A., Raymond, S. N., & Duncan, M. 2013, *Nature*, 493, 381, doi: [10.1038/nature11780](https://doi.org/10.1038/nature11780)
- Kaib, N. A., Raymond, S. N., & Duncan, M. J. 2011, *ApJL*, 742, L24, doi: [10.1088/2041-8205/742/2/L24](https://doi.org/10.1088/2041-8205/742/2/L24)
- Kaib, N. A., White, E. B., & Izidoro, A. 2018, *MNRAS*, 473, 470, doi: [10.1093/mnras/stx2456](https://doi.org/10.1093/mnras/stx2456)
- Kouwenhoven, M. B. N., Goodwin, S. P., Parker, R. J., et al. 2010, *MNRAS*, 404, 1835, doi: [10.1111/j.1365-2966.2010.16399.x](https://doi.org/10.1111/j.1365-2966.2010.16399.x)
- Kozai, Y. 1962, *AJ*, 67, 591, doi: [10.1086/108790](https://doi.org/10.1086/108790)
- Kroupa, P. 1995, *MNRAS*, 277, 1491, doi: [10.1093/mnras/277.4.1491](https://doi.org/10.1093/mnras/277.4.1491)
- Kroupa, P. 2001, in *The Formation of Binary Stars*, ed. H. Zinnecker & R. Mathieu, Vol. 200, 199
- Kroupa, P., & Burkert, A. 2001, *ApJ*, 555, 945, doi: [10.1086/321515](https://doi.org/10.1086/321515)
- Lada, C., & Lada, E. 2003, *Annual Reviews of A&A*
- Lam, C., & Kipping, D. 2018, *MNRAS*, 476, 5692, doi: [10.1093/mnras/sty022](https://doi.org/10.1093/mnras/sty022)
- Levison, H. F., Duncan, M. J., Brasser, R., & Kaufmann, D. E. 2010, *Science Magazine*, 329, doi: [10.1126/science.187535](https://doi.org/10.1126/science.187535)
- Malmberg, D., Davies, M. B., & Heggie, D. C. 2011, *MNRAS*, 411, 859, doi: [10.1111/j.1365-2966.2010.17730.x](https://doi.org/10.1111/j.1365-2966.2010.17730.x)
- Parker, R. J., & Goodwin, S. P. 2009, *MNRAS*, 397, 1041, doi: [10.1111/j.1365-2966.2009.15037.x](https://doi.org/10.1111/j.1365-2966.2009.15037.x)
- Parker, R. J., Goodwin, S. P., Kroupa, P., & Kouwenhoven, M. B. N. 2009, *MNRAS*, 397, 1577, doi: [10.1111/j.1365-2966.2009.15032.x](https://doi.org/10.1111/j.1365-2966.2009.15032.x)
- Plummer, H. C. 1911, *MNRAS*, 71
- Proszkow, E.-M., & Adams, F. C. 2009, *ApJS*, 185, 486, doi: [10.1088/0067-0049/185/2/486](https://doi.org/10.1088/0067-0049/185/2/486)
- Quarles, B., & Lissauer, J. J. 2018, *AJ*, 155, 130, doi: [10.3847/1538-3881/aaa966](https://doi.org/10.3847/1538-3881/aaa966)
- Rasio, F. A., & Ford, E. B. 1996, *Science*, 274, 954, doi: [10.1126/science.274.5289.954](https://doi.org/10.1126/science.274.5289.954)
- Reche, R., Beust, H., & Augereau, J. C. 2009, *A&A*, 493, 661, doi: [10.1051/0004-6361:200810419](https://doi.org/10.1051/0004-6361:200810419)
- Rein, H., & Liu, S. F. 2012, *A&A*, 537, A128, doi: [10.1051/0004-6361/201118085](https://doi.org/10.1051/0004-6361/201118085)
- Sadavoy, S. I., & Stahler, S. W. 2017, *Monthly Notices of the Royal Astronomical Society*, 469, 3881–3900, doi: [10.1093/mnras/stx1061](https://doi.org/10.1093/mnras/stx1061)
- Siraj, A., & Loeb, A. 2020, *ApJL*, 899, L24, doi: [10.3847/2041-8213/abac66](https://doi.org/10.3847/2041-8213/abac66)
- Turk, M. J., Abel, T., & O’Shea, B. 2009, *Science*, 325, 601, doi: [10.1126/science.1173540](https://doi.org/10.1126/science.1173540)
- Venner, A., Pearce, L. A., & Vanderburg, A. 2021, arXiv e-prints, arXiv:2111.03676. <https://arxiv.org/abs/2111.03676>
- Weidner, C., & Kroupa, P. 2004, *Monthly Notices of the Royal Astronomical Society*, 348, 187–191, doi: [10.1111/j.1365-2966.2004.07340.x](https://doi.org/10.1111/j.1365-2966.2004.07340.x)
- Wiegert, P. A., & Holman, M. J. 1997, *AJ*, 113, 1445, doi: [10.1086/118360](https://doi.org/10.1086/118360)
- Winn, J. N., Fabrycky, D., Albrecht, S., & Johnson, J. A. 2010, *The Astrophysical Journal*, 718, L145, doi: [10.1088/2041-8205/718/2/L145](https://doi.org/10.1088/2041-8205/718/2/L145)
- Wisdom, J., & Holman, M. 1991, *AJ*, 102, 1528, doi: [10.1086/115978](https://doi.org/10.1086/115978)